Fe I Oscillator Strengths for the Gaia-ESO Survey

M. P. Ruffoni[1]⋆, E. A. Den Hartog[2], J. E. Lawler[2], N. R. Brewer[2], K. Lind[3], G. Nave[4] and J. C. Pickering[1]

[1]*Blackett Laboratory, Imperial College London, London SW7 2BW, UK*
[2]*Department of Physics, University of Wisconsin, Madison, WI 53706, USA*
[3]*Institute of Astronomy, University of Cambridge, Cambridge CB3 0HA, UK*
[4]*National Institute of Standards and Technology, Gaithersburg, Maryland 20899-8422, USA*

ABSTRACT
The Gaia-ESO Public Spectroscopic Survey (GES) is conducting a large-scale study of multi-element chemical abundances of some 100 000 stars in the Milky Way with the ultimate aim of quantifying the formation history and evolution of young, mature and ancient Galactic populations. However, in preparing for the analysis of GES spectra, it has been noted that atomic oscillator strengths of important Fe I lines required to correctly model stellar line intensities are missing from the atomic database. Here, we present new experimental oscillator strengths derived from branching fractions and level lifetimes, for 142 transitions of Fe I between 3526 Å and 10864 Å, of which at least 38 are urgently needed by GES. We also assess the impact of these new data on solar spectral synthesis and demonstrate that for 36 lines that appear unblended in the Sun, Fe abundance measurements yield a small line-by-line scatter (0.08 dex) with a mean abundance of 7.44 dex in good agreement with recent publications.

Key words: atomic data — line: profiles — methods: laboratory — techniques: spectroscopic

1 INTRODUCTION

The Gaia-ESO Public Spectroscopic Survey (GES) is currently taking place at the European Southern Observatory (ESO), employing the Fibre Large Array Multi Element Spectrograph (FLAMES) instrument at the Very Large Telescope (VLT) facility. Its aim is to obtain high quality spectroscopy of some 100 000 stars from all major components of the Milky Way to quantify the "kinematic multichemical element abundance distribution functions of the Milky Way Bulge, the thick Disc, the thin Disc, and the Halo stellar components, as well as a very significant sample of 100 open clusters" (Gilmore et al. 2012). Over the course of the survey, chemical abundances will be measured for alpha and iron-peak elements in all stars with visual magnitude less than nineteen. These data will probe stellar nucleosynthesis by examining nuclear statistical equilibrium and the alpha-chain. Ultimately, the abundances and radial velocities will be combined with high-precision position and proper motion measurements from the European Space Agency's *Gaia* mission, to "quantify the formation history and evolution of young, mature and ancient Galactic populations" (Perryman et al. 2001). Gilmore et al. (2012) also state that "Considerable effort will be invested in abundance calibration and ESO archive re-analysis to ensure maximum future utility."

To achieve these high-level aims, it is vital that fundamental atomic data be available for lines in the GES spectral range:

⋆ E-mail:m.ruffoni@imperial.ac.uk

4800 Å to 6800 Å for measurements with the high-resolution FLAMES Ultraviolet and Visual Echelle Spectrograph (UVES) and 8500 Å to 9000 Å for measurements with the mid-resolution FLAMES *Giraffe* spectrograph. The availability of absorption oscillator strengths, f (usually used as the $\log(gf)$, where g is the statistical weight of the lower level), is particularly important for the correct modelling and analysis of stellar line intensities; especially so for abundant elements such as iron, which is also used to infer fundamental stellar parameters.

However, in preparing a list of iron lines to be targeted during the analysis of GES spectra, the GES line list team noted that of 449 well-resolved lines of neutral iron (Fe I) expected to be visible with sufficient signal-to-noise ratio, only 167 have published log(gf) values measured in the laboratory with uncertainties below 25 %. Experimental log(gf) values with large uncertainties (greater than 50 % in many cases) were available for an additional 162 lines. For the final 120 lines, no experimental $\log(gf)$s were available at all. A similar observation was made by Bigot and Thévenin (2006) for lines of interest to the *Gaia* mission.

As a result of this inadequacy in the atomic database, and similar inadequacies observed by other astronomers (see Ruffoni et al. (2013a) and Pickering et al. (2011), for example), we have undertaken a new study of the Fe I spectrum with the aim of providing accurate $\log(gf)$ values for lines of astrophysical significance. In Section 3 of this paper, we report accurate $\log(gf)$s for 142 Fe I lines, 64 of which have been measured experimentally for the first

time. The $\log(gf)$ values of at least 38 of these lines are urgently needed for the GES survey.

2   EXPERIMENTAL PROCEDURE

Typically, $\log(gf)$s are obtained in the laboratory from measurements of atomic transition probabilities, A, (Thorne at al. 2007).

$$\log(gf) = \log\left[A_{ul}g_u\lambda^2 \times 1.499 \times 10^{-14}\right], \tag{1}$$

where the subscript u denotes a target upper energy level, and ul, a transition from this level to a lower level, l, that results in emission of photons of wavelength λ (nm). g_u is the statistical weight of the upper level. The A_{ul} values are found by combining experimental branching fractions, BF_{ul}, with radiative lifetimes, τ_u (Huber and Sandeman 1986).

$$A_{ul} = \frac{BF_{ul}}{\tau_u} ; \quad \tau_u = \frac{1}{\sum_l A_{ul}}. \tag{2}$$

The BF_{ul} for a given transition is the ratio of its A_{ul} to the sum of all A_{ul} associated with u. This is equivalent to the ratio of observed relative line intensities in photons/s for these transitions.

$$BF_{ul} = \frac{A_{ul}}{\sum_l A_{ul}} = \frac{I_{ul}}{\sum_l I_{ul}}. \tag{3}$$

This approach does not depend on any form of equilibrium in the population distribution over different levels, but it is essential that all significant transitions from u be included in the sum over l.

The BFs measured for this work were extracted from Fe I spectra acquired by Fourier transform (FT) spectroscopy, as described in Section 2.1. The radiative lifetimes required to solve Equation 2 were obtained through laser induced fluorescence (LIF), and are discussed in Section 2.2.

2.1   Branching Fraction Measurements

The BFs reported here were obtained from Fe I emission line spectra measured in two overlapping spectral ranges between 8200 cm^{-1} and 35500 cm^{-1} (between 1220 nm and 282 nm), labelled A and B in Table 1.

Spectrum A was measured between 8200 cm^{-1} and 25500 cm^{-1} (3920.5 Å and 12191.8 Å) on the 2 m Fourier transform (FT) spectrometer at the National Institute of Standards and Technology (NIST) (Nave et al. 1997). The Fe I emission was generated from an iron cathode mounted in a water cooled hollow cathode lamp (HCL) running at a current of 2.0 A in a Ne atmosphere of 370 Pa pressure. The response of the spectrometer as a function of wavenumber was obtained by measuring the spectrum of a calibrated tungsten (W) halogen lamp with spectral radiance known to ±1.1 % between 250 nm and 2400 nm. W lamp spectra were acquired both before and after measurements of the Fe/Ne HCL spectrum to verify that the spectrometer response remained stable.

220 individual Fe/Ne HCL spectra were acquired over two days and coadded to improve the signal-to-noise ratio of weak lines. However, due to different detector configurations being used on each day, the spectrometer response function varied significantly between the two. As a result, the files Fe080311.001 to .003 (containing 110 spectra, acquired with a Si photodiode on each outputs of the FT spectrometer) were coadded and intensity calibrated using the spectral response function labelled "Spectrum A (1)" in Figure 1, while Fe080411_B.001 to .003 (containing the remaining 110 spectra, acquired with a single Si photodiode mounted on

the unbalanced output of the FT spectrometer) were coadded and calibrated using the response function labelled "Spectrum A (2)". These response functions were obtained with the aid of the FAST package (Ruffoni 2013b). The two intensity calibrated line spectra were then themselves coadded to produce the final spectrum.

Spectrum B was measured between 20000 cm^{-1} and 35500 cm^{-1} (2816.1 Å and 4998.6 Å) on the Imperial College VUV spectrometer (Thorne et al. 1996), which is based on the laboratory prototype designed by Thorne et al. (1987). The Fe emission was generated from an iron cathode mounted in a new HCL designed and manufactured at Imperial College London (IC). The lamp was operated at 700 mA in a Ne atmosphere of 170 Pa pressure to provide reasonable signal-to-noise ratio in the weaker lines while avoiding self-absorption effects in the stronger lines.

The spectrometer response function for spectrum B is also shown in Figure 1, and was again obtained from a calibrated W lamp, measured before and after each Fe/Ne HCL measurement. Uncertainties in the relative spectral radiance of the W lamp used at IC, and calibrated by the National Physical Laboratory (NPL), do not exceed ±1.4 % between 410 nm and 800 nm, and rise to ±2.8 % at 300 nm.

Many of the upper energy levels studied here are linked to transitions that produced spectral lines contained entirely within the range of either spectrum A or B. In these cases, all branching fractions pertaining to those levels were derived from a single spectrum. Where lines associated with a given upper level spanned both spectra, their intensities were put on a common relative scale by comparing the intensity of lines in the overlap region between the two spectra. The process of intensity calibrating overlapping spectra is discussed in detail in Pickering et al. (2001a) and Pickering et al. (2001b).

For each target upper level, the predicted transitions to lower levels were obtained from the semi-empirical calculations of Kurucz (2007). Emission lines from these transitions were then identified in our Fe spectra, and the XGremlin package (Nave et al. 1997) used to fit Voigt profiles to those that were observed above the noise limit. The residuals from each fit were examined to ensure that the observed line profiles were free from self-absorption and not blended with other features.

The spectra and fit results from XGremlin were then loaded into the FAST package (Ruffoni 2013b), where the BFs for each observed target line were measured. Lines which were too weak to be observed – typically those predicted by Kurucz (2007) to contribute less than 1 % of the total upper level BF – were not considered, as were lines that were either blended or outside the measured spectral range. Their predicted contribution to the total BF was assigned to a 'residual' value, which was used to scale the sum over l of the measured line intensity, I_{ul}, in Equation 3.

The calculation of experimental uncertainties in BFs measured by FT spectroscopy with FAST has been discussed in our recent papers (Ruffoni et al. 2013a; Ruffoni 2013b). The uncertainty in a given BF, ΔBF_{ul}, is

$$\left(\frac{\Delta BF_{ul}}{BF_{ul}}\right)^2 = (1-2BF_{ul})\left(\frac{\Delta I_{ul}}{I_{ul}}\right)^2 + \sum_{j=1}^{n} BF_{uj}^2 \left(\frac{\Delta I_{uj}}{I_{uj}}\right)^2, \tag{4}$$

where I_{ul} is the calibrated relative intensity of the emission line associated with the electronic transition from level u to level l, and ΔI_{ul} is the uncertainty in intensity of this line due to its measured signal-to-noise ratio and the uncertainty in the intensity of the standard lamp. From Equation 2, it then follows that the uncertainty in A_{ul} is

Table 1. FTS spectra taken for BF measurements.

Spectrum	Wavenumber[a] Range (cm^{-1})	Detector	Filter	Resolution (cm^{-1})	Spectrum Filename[b]
A (NIST)	8200 - 25500	Si photodiode	None	0.02	Fe080311.001 to .003; Fe080411_B.001 to .003 (220 coadds)
B (IC)	20000 - 35500	Hammamatsu R11568 PMT	Schott BG3	0.037	Fe130610.002 to .047 (96 coadds)

Note: The identification of commercial products does not imply recommendation or endorsement by the National Institute of Standards and Technology, nor does it imply that the items identified are necessarily the best available for the purpose.

[a] The equivalent wavelength ranges are: Spectrum A: λ = 3920.5 Åto 12191.8 Å, Spectrum B: λ = 2816.1 Åto 4998.6 Å.

[b] The named spectra were coadded to improve the signal-to-noise ratio of weak lines.
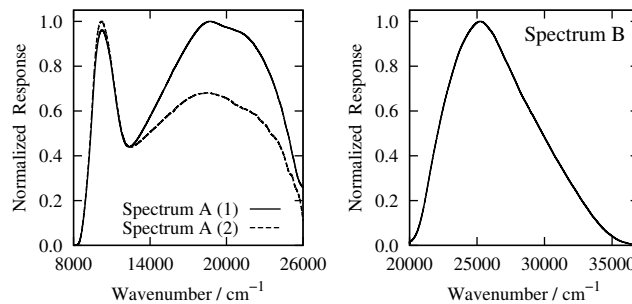
Figure 1. Instrument response functions used to intensity calibrate the two FT spectra listed in Table 1.

$$\left(\frac{\Delta A_{ul}}{A_{ul}}\right)^2 = \left(\frac{\Delta \mathrm{BF}_{ul}}{\mathrm{BF}_{ul}}\right)^2 + \left(\frac{\Delta \tau_{ul}}{\tau_{ul}}\right)^2, \qquad (5)$$

where $\Delta \tau_{ul}$ is the uncertainty in our measured upper level lifetime. Finally, the uncertainty in $\log(gf)$ of a given line is

$$\Delta \log(gf) = \log\left(1 + \frac{\Delta A_{ul}}{A_{ul}}\right), \qquad (6)$$

2.2 Upper Level Radiative Lifetimes

Radiative lifetimes are measured to ± 5 % using time-resolved laser-induced fluorescence (LIF) on an atomic beam of iron atoms. A diagram of the apparatus is shown in O'Brian et al. (1991). The beam is produced by sputtering iron atoms in a hollow cathode discharge. The electrical discharge is operated in ≈ 50 Pa argon gas. A DC current of ≈ 30 mA maintains the discharge between ≈ 10 A, 10 µs duration pulses at 30 Hz repetition rate. The hollow cathode, which is lined with a foil of pure iron, is closed on one end except for a 1 mm hole which is flared on one side to act as a nozzle. Energetic argon ions accelerated through the cathode fall potential efficiently sputter the iron from the surface of the cathode. The iron atoms (neutral as well as singly-ionized) are differentially pumped through the nozzle amidst a flow of argon gas into a low pressure (10^{-2} Pa) scattering chamber. This "beam" is slow (neutrals are moving $\sim 5 \times 10^4$ cm/s and ions somewhat faster) and weakly collimated.

Measurement of the odd-parity level lifetime required single-step laser excitation. In this technique the atomic beam is intersected at right angles by a single beam from a nitrogen laser-pumped dye laser 1 cm below the nozzle. The delay between the discharge pulse and the laser pulse is adjustable, and optimized typ-

ically at ~ 20 µs, which corresponds to the average transit time of the iron atoms. The scattering volume is at the center of a set of Helmholtz coils which zeroes the magnetic field to within ± 2 µT. This very low field ensures that the excited iron atoms do not precess about the Earth's magnetic field, thus eliminating the potential for Zeeman quantum beats in the fluorescence. The dye laser is tunable over the range 205 nm to 720 nm using a large selection of dyes as well as frequency doubling crystals. It has a bandwidth of ~ 0.2 cm^{-1}, a half-width duration of ~ 3 ns and, more importantly for this work, terminates completely in a few ns. The laser allows for selective excitation of the level under study, eliminating the problem of cascade from higher-lying levels that plagued earlier, non-selective techniques. The laser is tuned to a transition between the ground state or a low-lying metastable level and the level under study. Identifying the correct transition is non-trivial, particularly for a dense, line rich spectrum such as Fe I and Fe II. The laser is tuned to within ≈ 0.1 nm of the transition by adjusting the angle of the grating, which is the tuning element of the laser, while measuring the wavelength with a 0.5 m monochromator. A LIF spectrum of 0.5 nm to 1.0 nm range is then recorded using a boxcar averager by slowly changing the pressure in an enclosed volume surrounding the grating. Pressure scanning provides exceptional linearity and reproducibility. The pressure scanned spectrum is then compared to the published linelist from the NIST database[1] to correctly identify the line of interest.

Fluorescence is collected in a direction mutually orthogonal to the atomic and laser beams through a pair of fused-silica lenses comprising an f/1 optical system. A spectral filter, either a broadband colored-glass filter or a narrowband multilayer dielectric filter, is inserted between the two lenses where the fluorescence is

[1] http:// physics.nist.gov/PhysRefData/ASD/index.html

approximately collimated. The filter is chosen to maximize fluorescence throughput while reducing or eliminating scattered laser light and eliminating possible cascade from lower-lying levels. Fluorescence is focused onto the photocathode of a RCA 1P28A photomultiplier tube (PMT) and the PMT signal is recorded using a Tektronix SCD1000 transient digitizer. The bandwidth of the PMT, digitizer and associated electronics is adequate to measure lifetimes down to $\sim$2 ns. The lifetimes reported here are in the 10 ns to 25 ns range and are well within the bandwidth limits. The characteristics of this PMT, i.e. fast rise time and high spectral response in the UV and visible, are favourable for radiative lifetime measurements.

The digitizer is triggered with the signal from a fast photodiode which is illuminated by light picked off from the nitrogen laser. Recording of the fluorescence by the digitizer is delayed until after the dye laser pulse has completely terminated, making deconvolution of the laser temporal profile and fluorescence signals unnecessary. Each data record consists of an average of 640 fluorescence decays followed by an average of 640 background traces with the laser tuned off-line. The data is divided into an early time and a late time interval for analysis. A linear least-square fit to a single exponential is performed on the background subtracted fluorescence decay to determine a lifetime for each interval. Comparison of the lifetimes in the two intervals is a sensitive indicator of whether the decay is a clean exponential or whether some systematic effect has rendered it non-exponential. Five of these decay times are averaged together to determine the lifetime. The lifetime of each odd-parity level is measured twice, using two different laser transitions. This redundancy helps to ensure that the transition is classified correctly, free from blends, and is identified correctly in the experiment.

Measurement of the even-parity levels reported here required two-step laser excitation. The introduction of a second laser results in an added layer of complexity in the excitation of the level and timing of the experiment, as well as more stringent requirements for the filtering of the fluorescence. The fluorescence detection, recording and analysis is identical to the one-laser experiment. While it is possible to pump two dye lasers using one nitrogen laser, this limits the power available in either laser beam. Instead, we used two dye lasers each with its own nitrogen laser pump. The delay generator which, in the one laser experiment is used to trigger the laser $\sim$20 μs after the discharge pulse, is in this case used to trigger a second dual gate generator that has very precise timing ($\pm$1 ns) between its two gates. These gates are used to trigger the two nitrogen lasers which pump the dye lasers. Because the two nitrogen lasers have different thyratron charging and firing mechanisms, there is a substantial amount of timing jitter (approximately $\pm$20 ns) between the resulting dye laser pulses. This jitter results in some additional shot-to-shot fluctuation in the final measurement as the population in the intermediate level has decayed more or less from its peak. The lifetimes of all the intermediate levels used but one is substantially longer than this jitter (60 ns to 85 ns as measured by O'Brian et al. (1991)), so the added shot-to-shot noise was not severe. Even the measurement with the short-lived (9.6 ns as measured by O'Brian et al. (1991)) intermediate level had only $\sim$2 % statistical scatter in the final average. The delay between the two lasers is adjusted such that the laser which drives the transition from the intermediate level to the even-parity level being studied (laser 2) arrives on average $\sim$20 ns after that which drives a transition between the ground or low-lying metastable level and an intermediate odd-parity level (laser 1). The trigger signal for the boxcar and digitizer was from the fast photodiode illuminated with light from the laser 2 nitrogen laser.

The two lasers are sent through the scattering chamber at slight angles relative to each other, such that they intersect in the viewing volume. Once laser 1 is tuned onto the appropriate transition to drive the intermediate level, it is left there for the duration of the measurement. A narrowband, multilayer dielectric filter is inserted in the collection optics which completely blocks fluorescence from the intermediate level but transmits fluorescence from the upper level. Laser 2 was tuned on and off the transition to provide the fluorescence and background traces as in the one-step experiment. The fluorescence was observed to go away when either laser 1 or laser 2 was blocked and the other laser was allowed to pass through the system, ensuring that it was indeed from a two-step process. This provides the assurance that the correct lifetime is being measured that a redundant measurement gives in the one-step experiment. Each two-step lifetime was therefore measured only once.

Systematic effects such as Zeeman quantum beats and bandwidth limits are well-studied and controlled in the experiment. Another effect, the flight out of view effect, is caused by atoms leaving the viewing volume before fluorescing. This effect is only a problem for long lifetimes, greater than 300 ns for neutrals and greater than 100 ns for ions, and is not a problem for the current set of lifetimes. In addition to understanding and minimizing these systematics, we also regularly measure a set of benchmark lifetimes, to compare our measured values to the known lifetimes. These benchmarks are lifetimes that are either very well known from theoretical calculations, or from an experiment which has significantly smaller and generally different systematic uncertainties from our own. For the current set of lifetimes, we measured three benchmarks which approximately bracketed the range of values reported here. These are: $2p\ ^2P_{3/2}$ level of singly ionized Be at 8.8519(8) ns (variational method calculation (Yan et al. 1998)); the $3p\ ^2P_{3/2}$ level of neutral Na at 16.23(1) ns (accuracy of $\leqslant$ 0.1 % at 90 % confidence level) taken from the recent NIST critical compilation of Kelleher & Podobedova (2008); and the $2p_2\ 4p'[1/2]_1$ level of neutral Ar at 27.85(7) ns (beam-gas-laser-spectroscopy (Volz & Schmoranzer 1998)). Benchmarks are measured in exactly the same way as the Fe I lifetimes except that the cathode lining is changed in the cases of the Be$^+$ and Na measurements. With these benchmarks we are able to quantify and make small corrections for any residual systematic effects ensuring that our final results are well within the stated uncertainty of $\pm$5 %. A recent comparison of LIF measurements in Sm II by Lawler et al. (2008) suggests that the $\pm$5 % is a conservative estimate of the lifetime uncertainty.

The lifetime results are given in Table 2. A total of 1 odd-parity and 8 even-parity level lifetimes were measured; most for the first time. The even-parity e^5D_4 level at 44677.003 cm^{-1} was also measured by Marek et al. (1979) using delayed coincidence detection after laser excitation, and agrees with our lifetime to about $\pm$1 %. This good level of agreement is what we have come to expect between modern, laser-based methods.

3   RESULTS

Table 2 lists the Fe I upper levels that were targeted in this study. They were selected because their branches to lower levels produce many spectral lines of interest to the GES survey that currently have either no experimentally measured $\log(gf)$ value in the literature, or a $\log(gf)$ known to worse than $\pm$25%. We also included two levels, those at 43633.530 cm^{-1} and 51461.667 cm^{-1}, for which accurate lifetimes and $\log(gf)$s were reported by O'Brian et al. (1991). These served primarily as a means to check the accuracy of $\log(gf)$s produced with the aid of the FAST code, but in re-

Table 2. Radiative lifetimes for Fe I levels used to derive the $\log(gf)$s in Table 3. The uncertainty in both our lifetime measurements and those of O'Brian et al. (1991) was ± 5 %.

Configuration	Term	J	Upper Level (cm^{-1})	Upper Level (eV)	Intermediate Level (cm^{-1})	Laser Wavelengths[a] Step 1 (nm)	Laser Wavelengths[a] Step 2 (nm)	Observation Wavelength[b] (nm)	Our Lifetime (ns) ± 5 %	Previous Lifetime (ns) ± 5 %
Radiative lifetime for odd parity Fe I levels using single step excitation.										
$3d^6(^3\mathrm{H})4s4p(^3\mathrm{P}^o)$	y^{1}G^o	4	48702.532	6.0383441		241.906, 414.341			21.0	
Radiative lifetimes for even parity Fe I levels using 2-step excitation.										
$3d^6(^5\mathrm{D})4s(^6\mathrm{D})5s$	e^{5}D	4	44677.003	5.5392422	25899.987	385.991	532.418	561	15.4	15.6 ± 0.9^c
$3d^7(^4\mathrm{F})5s$	e^{5}F	4	47377.952	5.8741171	26140.177	382.444	470.727	490	19.9	
$3d^7(^4\mathrm{F})5s$	e^{3}F	4	47960.937	5.9463981	26140.177	382.444	458.151	600	22.1	
$3d^6(^5\mathrm{D})4s(^4\mathrm{D})5s$	e^{3}D	3	51294.217	6.3596721	26140.177	382.444	397.438	500	9.9	
$3d^6(^5\mathrm{D})4s(^4\mathrm{D})5s$	g^{5}D	3	51770.554	6.4187304	26140.177	382.444	390.052	408	12.1	
$3d^6(^5\mathrm{D})4s(^4\mathrm{D})5s$	e^{3}D	1	52039.889	6.4521236	26339.694	385.637	388.992	500	10.4	
$3d^6(^5\mathrm{D})4s(^6\mathrm{D})4d$	e^{5}P	2	52067.466	6.4557907	26140.177	382.444	385.585	446	14.3	
$3d^7(^4\mathrm{F})4d$	f^{3}F	4	54683.318	6.7798670	36686.174	404.581	555.489	570	23.5	
Additional radiative lifetimes from O'Brian et al. (1991).										
$3d^6 4s(^6\mathrm{D})5s$	e^{7}D	4	43163.323	5.3515698		423.59 427.12				8.5
$3d^6 4s(^6\mathrm{D})5s$	e^{7}D	2	43633.530	5.4098680		418.70 423.36				8.4
$3d^6 4s(^6\mathrm{D})4d$	f^{5}F	4	51461.667	6.3804332		315.32				12.7

Note: The configuration, term, and energy level data are taken from Nave et al. (1994).

[a] Laser wavelengths are from the NIST Atomic Spectra Database (http://www.nist.gov/pml/data/asd.cfm).
[b] Fluorescence was observed through ~ 10 nm bandpass multi-layer dielectric filters. The filter angle was adjusted where needed to centre the bandpass at the indicated wavelength.
[c] Marek et al. (1979).

measuring them we were also able to improve upon the experimental uncertainty achieved by O'Brian et al. (1991) and provide $\log(gf)$s for a number of weaker branches not included in their paper. Some further lines reported by O'Brian et al. (1991) appear in branches from other upper levels, as do a few lines for which accurate $\log(gf)$s were reported by Blackwell et al. (1982) and Bard et al. (1991). Again, these served as a means to check the accuracy of our results.

Our measured branching fractions, transition probabilities, and $\log(gf)$s are listed in Table 3 along with the most accurate $\log(gf)$s previously available in the literature. The lower level terms, and transition vacuum wavenumbers and air wavelengths were taken from Nave et al. (1994), where possible. For the small number of lines not included in Nave et al. (1994), the transition vacuum wavenumber and air wavelength shown were obtained from our FT spectra by calibrating the measured wavenumber scale to match the calibrated scale used by Nave et al. (1994). These lines are marked in Table 3 by a '*' in the Lower Level column.

Table 3 is sorted in order of ascending transition wavenumber, with lines grouped by common upper level energy. For each set of lines, the upper level energy, configuration, term, and J value, and measured lifetime are given as a header row. The unobserved 'residual' BF, described in Section 2.1, is given in the BF column at the end of each set. The lines that contribute to these residuals are given in Table 4 where they have either been observed in previous studies, or predicted by Kurucz (2007) to contribute more than 1 % to the total BF. Reasons for their omission in this study are given.

For six of the eleven upper levels (those at 43633.530 cm^{-1}, 44677.003 cm^{-1}, 47377.952 cm^{-1}, 47960.937 cm^{-1}, 48702.532 cm^{-1}, and 51294.217 cm^{-1}) the residual BF amounted to less than 5%, and arose solely from lines predicted by Kurucz (2007) to contribute to the total set of branches that were too weak to be observed experimentally. For the remaining five levels (those at 51461.667 cm^{-1}, 51770.554 cm^{-1}, 52039.889 cm^{-1}, 52067.446 cm^{-1}, and 54683.318 cm^{-1}) a large majority of branches were observed, but at least one stronger line was unavailable due to being unobserved above the spectral noise, blended with another line, or significantly separated in wavenumber from the rest of the branches (which prevents correct intensity calibration). In all cases, the missing BF was taken from previously published values, if they existed, or from Kurucz's calculations otherwise, as shown in Table 4. Any error in these values will affect the overall normalisation of $\log(gf)$s for the level in question, in turn leading to a systematic error in their value. However, we expect this error to be small, and so have neglected it, for two reasons. Firstly, there is good agreement between our $\log(gf)$s and those from O'Brian et al. (1991) for branches from the 51461.667 cm^{-1} level, which has a residual BF of 0.124 (the largest of all levels) and secondly, this residual can be varied by as much as ± 20% without the normalisation error exceeding the random uncertainty in $\log(gf)$ of any of the branches.

Lines that are of particular interest for the GES survey are marked in Table 3 in the "GES Target?" column. In some cases the $\log(gf)$s for these lines have been measured in earlier studies, in which case we have sought to reduce their uncertainty. For lines

originally measured by May et al. (1974), the quoted published $\log(gf)$s are the corrected values given by Fuhr and Wiese (2006) in their recent critical compilation of Fe I $\log(gf)$s. In preparing their compilation, these authors noted that the lifetimes used by May et al. (1974) originate from data produced in the 1960s and early 1970s. Comparing these to the cascade-free LIF lifetimes measured by O'Brian et al. (1991), they found that for 13 energy levels between $52000\ \mathrm{cm}^{-1}$ and $57000\ \mathrm{cm}^{-1}$ the lifetimes given by O'Brian et al. (1991) were systematically shorter by about 20%, most likely due to the absence of cascade effects. For levels below $36000\ \mathrm{cm}^{-1}$, this systematic error vanished. Fuhr and Wiese (2006) therefore corrected the $\log(gf)$s given by May et al. (1974) for levels above $36000\ \mathrm{cm}^{-1}$ to make them consistent with the lifetime data of O'Brian et al. (1991). For the remaining $\log(gf)$s, Fuhr and Wiese (2006) found fair agreement with the results of O'Brian et al. (1991) and Blackwell et al. (1982) where they overlapped. However, the scatter was "quite large", suggesting that the uncertainties given by May et al. (1974) should be significantly larger. In Table 3, the uncertainties in $\log(gf)$s from May et al. (1974) are therefore given as a letter 'D' or 'E' to follow the notation used by Fuhr and Wiese (2006). A letter 'D' indicates that the uncertainty is likely to be up to 50%, whereas an 'E' indicates a probable uncertainty greater than 50%, but within a factor of two in most cases.

Figure 2 shows a comparison between our new $\log(gf)$s and those published previously. The top panel shows the difference between our values and those reported by O'Brian et al. (1991), Blackwell et al. (1982), and Bard et al. (1991). The long dashed, short dashed and dotted horizonatal lines indicate uncertainties of ± 2 %, ± 10 % and ± 25 %, respectively, corresponding to uncertainties coded ' A', 'B' and 'C' by Fuhr and Wiese (2006). The work of Blackwell et al. (1982) continues to serve as a gold-standard for Fe I $\log(gf)$s in the literature. Five lines from their study are also included our work, and the $\log(gf)$ for each agrees within their combined experimental uncertainty of ± 5%. There is also very good agreement with the results of O'Brian et al. (1991) and Bard et al. (1991). 25 of the 29 $\log(gf)$s from these papers agree within the combined experimental uncertainties with no discernible systematic offset between the published results and our new values. Together, these testify to the general accuracy of our $\log(gf)$ measurements and the accuracy of the FAST code in extracting $\log(gf)$s from FT spectra.

The lower panel of Figure 2 shows the difference between our values and the corrected $\log(gf)$s given by Fuhr and Wiese (2006) for the data reported by May et al. (1974). The dashed and dotted lines this time indicate uncertainties of ± 50 % and ± 100 %, respectively, which correspond to uncertainties coded 'D' and 'E' by Fuhr and Wiese (2006). 31 of the 39 corrected $\log(gf)$s from May et al. (1974) agree with our new values when considering the enlarged uncertainties attributed to them by Fuhr and Wiese (2006), but there is considerable scatter in the results, as was also noted by Fuhr and Wiese (2006). There is also a systematic offset of $\log(gf)_{(New-Pub)} = 0.12$ for these lines. Our new $\log(gf)$s for these lines are accompanied by considerably smaller uncertainties; typically less than 25%, with some as low as 5% for stronger lines.

4   IMPACT ON SOLAR SPECTRAL SYNTHESIS

The Sun offers an excellent test-bed for new atomic data, with its high-resolution spectrum (Kurucz et al. 1984) and accurately
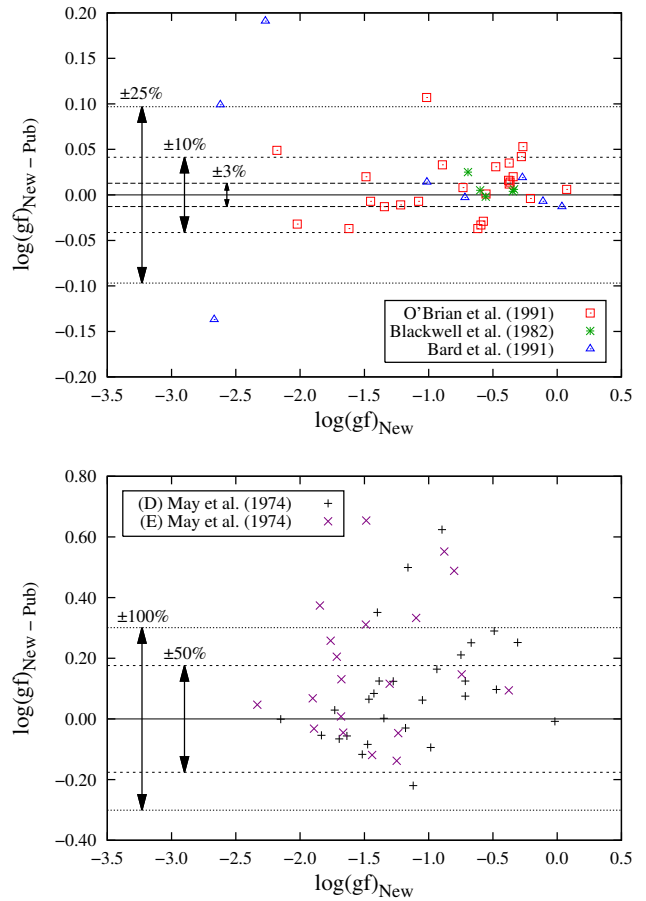
Figure 2. A comparison between the log(gf)s of this work and those already in the literature. The upper panel shows results from O'Brian et al. (1991), Blackwell et al. (1982), and Bard et al. (1991), which agree well with our new log(gf) values. The lower pane shows the corrected results from May et al. (1974), which have a considerably lower accuracy.

known fundamental parameters ("The Astronomical Almanac" 2013). To assess the impact of our new $\log(gf)$s on stellar syntheses, and also verify their general accuracy, we have determined line-by-line solar Fe abundances for a subset of 36 lines listed in Table 3 using both our new $\log(gf)$s and the best previously published values that are not of astrophysical nature. These lines, shown in Table 5, were selected as they are blend-free at the spectral resolution of the Kitt Peak Fourier Transform Spectrometer ($R \approx 200000$) flux atlas (Kurucz et al. 1984), and are accompanied by good broadening parameters and accurate continuum placement. The synthesis and abundance determination were performed under the assumption of local thermodynamic equilibrium (LTE), with the one dimensional, plane-parallel radiative transfer code SME (Valenti & Piskunov 1996), using a MARCS model atmosphere (Gustafsson et al. 2008).

We adopted a solar effective temperature $T_{\mathrm{eff}} = 5777\,K$, a surface gravity $\log(grav.) = 4.44$, a microturbulence of $\xi_{\mathrm{vmic}} = 1.0\,\mathrm{km\,s^{-1}}$, and a projected rotational velocity of $v_{\mathrm{rot}}\sin(i) = 2.0\,\mathrm{km\,s^{-1}}$. The radial-tangential macro-turbulence velocity, ξ_{vmac}, was varied between $1.5\,\mathrm{km\,s^{-1}}$ and $2.5\,\mathrm{km\,s^{-1}}$ to match the observed profile. The instrumental profile was assumed to be Gaussian. The line profiles were fitted individually using χ^2-
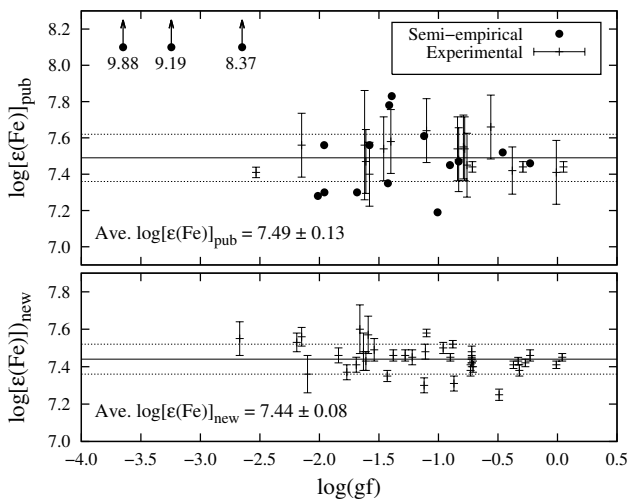
Figure 3. Solar metalicity, $\log[\epsilon(\text{Fe})]$, obtained from the synthesis of individual lines listed in Table 3 using the $\log(gf)$ values from this work, $\log(gf)_{\text{New}}$, and the best previously published values, $\log(gf)_{\text{Pub}}$. Only those lines that appear unblended in the solar spectrum are included. The three points at the top-left of the upper pane are discrepant semi-empirical values that lie outside the plotted range at the values shown. They were not included in the calculation of the average $\log[\epsilon(\text{Fe})]_{\text{Pub}}$.

minimisation between observed and synthetic spectra and varying the iron abundance.

The results are shown in Figure 3, where the abundances are plotted as a function of $\log(gf)$ on the standard astronomical scale.

$$\log[\epsilon(\text{Fe})] = \log_{10}\left[\frac{N(\text{Fe})}{N(\text{H})}\right] + 12 , \qquad (7)$$

where $N(\text{Fe})$ and $N(\text{H})$ are the number of iron and hydrogen atoms per unit volume, respectively.

Reassuringly, the new experimental data result in a small line-to-line scatter $(0.08 \text{ dex})^2$ and a mean abundance of 7.44, which is in good agreement with recent publications, such as 7.43 ± 0.02 from Bergemann et al. (2012) (MARCS, LTE result). In contrast, the best previously published values (omitting the discrepant semi-empirical values shown in Figure 3) produce an abundance of 7.49 ± 0.13, with the significantly larger scatter driven by the lines with no previous laboratory measurements. The observed and best-fit synthetic profiles of three of these lines are shown in Figure 4. They all fall within the GES wavelength windows, and two of them are also in the near-infrared *Gaia* Radial Velocity Spectrometer window (Katz et al. 2004).

Other lines with significant improvements in the solar modelling, but not shown in Table 5, are those at 4079.2 Å, 4933.9 Å, and 5171.7 Å, which are partly blended with astrophysically interesting lines such as the Ba II 4934.0 Å line, the Mn I 4079.2 Å line, and the Mg-I triplet line at 5172.7 Å.

5 SUMMARY

In Table 3, we have provided new $\log(gf)$ values for 142 Fe I lines from 12 upper levels, which include 38 lines of particular interest for the analysis of stellar spectra obtained by the GES survey.

---

[2] The unit dex stands for decimal exponent. x dex $= 10^x$.

Where $\log(gf)$s existed for these lines in the literature, we have found good agreement with our new values, which in many cases have smaller experimental uncertainties than those previously reported. This is especially true for uncertainties in $\log(gf)$s from May et al. (1974), which have been reduced from 50% or more to less than 25% in most cases.

This work represents part of an on-going collaboration between Imperial College London, U. Wisconsin, and NIST to provide the astronomy community with Fe I $\log(gf)$ values needed for the analysis of astrophysical spectra. Further publications will follow in the near future.

REFERENCES

Anstee S.D., O'Mara B.J., 1991, Mon. Not. R. Astron. Soc., 253, 549

Anstee S.D., O'Mara B.J., 1995, Mon. Not. R. Astron. Soc., 276, 859

Bard A., Kock A., Kock M., 1991, Astron. Astrophys., 248, 315

Bergemann M., Lind K., Collet R., Magic Z. & Asplund M., 2012, Mon. Not. R. Astron. Soc., 427, 27

Bigot L. & Thévenin F. 2006, Mon. Not. R. Astron. Soc., 372, 609

Blackwell D. E., Petford A. D., Shallis M. J., Simmons G.J., 1982, Mon. Not. R. Astron. Soc., 199, 43

Fuhr J. R., Wiese W. L. 2006, J. Phys. Chem. Ref. Data, 35, 1669

Gilmore G., Randich S., Asplund M., et al., 2012, Messenger, 147, 25

Gray D. F., 2005, "The Observation and Analysis of Stellar Photospheres" 3rd Ed., Chapter 11

Gustafsson B., Edvardsson B., Eriksson K., Jørgensen U. G., Nordlund Å. & Plez B., 2008, Astron. Astrophys., 486, 951

Huber M. C. E., Sandeman R. J., 1986, Rep. Prog. Phys., 49, 397

Katz D., Munari U., Cropper M., Zwitter T., Thévenin F., David M., et al., 2004, Mon. Not. R. Astron. Soc., 354, 1223

Kelleher D. E., Podobedova L. I., 2008, J. Phys. Chem. Ref. Data, 37, 267

Kurucz R. L., Furenlid I., Brault J. & Testerman L., 1984, "Solar flux atlas from 296 to 1300 nm", National Solar Observatory Atlas (Sunspot, NM: National Solar Observatory)

Kurucz R. L. 2007, http://kurucz.harvard.edu/atoms/2700/

Lawler J. E., Den Hartog E. A., Sneden C., Cowan, J. J., 2008, Can. J. Phys., 86, 1033
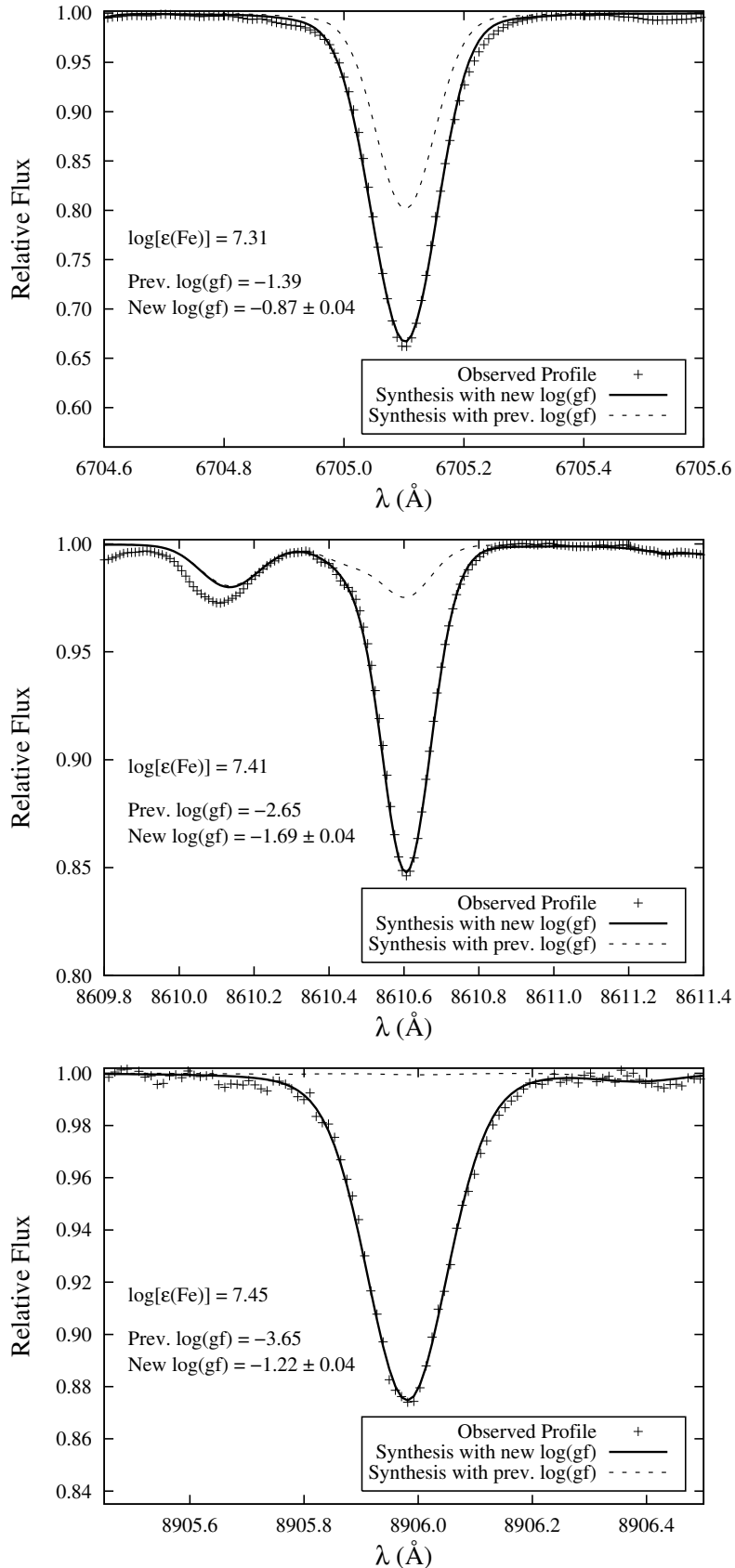
Figure 4. Three examples of lines observed in the solar spectrum and synthesised using both the $\log(gf)$s from this work and the best previously published values. The solid lines show the synthetic profiles obtained using the $\log(gf)$s from this work and the quoted values of $\log[\epsilon(\text{Fe})]$. The dashed lines show the synthetic profiles obtained using the same values of $\log[\epsilon(\text{Fe})]$, but adopting the best previously published $\log(gf)$s, shown in Table 5.

Marek J., Richter J., Stahnke H. J., 1979, Phys. Scr., 19, 325

May M., Richter J., Wichelmann J., 1974, Astron. Astrophy. Suppl. Ser., 18, 405

Nave G., Johansson S., Learner R. C. M., Thorne A. P., Brault J. W., 1994, ApJS, 94, 221

Nave G., Sansonetti C. J., Griesmann U., 1997, in OSA Technical Digest Ser. Vol. 3, Fourier Transform Spectroscopy, Optical Society of America, Washington DC, p. 38

O'Brian T. R., Wickliffe M. E., Lawler J. E., Whaling W., Brault J. W., 1991, J. Opt. Soc. Am. B, 8, 1185

Perryman M. A. C., de Boer K. S., Gilmore G., Høg E., Lattanzi M. G., Lindegren L., Luri X., Mignard F., Pace O., de Zeeuw P. T., 2001, A & A, 369, 339

Pickering J. C., Johansson S., Smith P. L., 2001a, A & A, 377, 361

Pickering J. C., Thorne A. P., Perez R., 2001b, ApJS, 132, 403

Pickering J. C., Blackwell-Whitehead R., Thorne A. P., Ruffoni M.P., Holmes C.E., 2011, Can. J. Phys., 89, 387

Ruffoni M. P., Allende-Prieto C., Nave G., Pickering J. C. 2013a, ApJ, 779, 17

Ruffoni M. P., 2013b, Comp. Phys. Comm., 184, 1770

Thorne A. P., Harris C. J., Wynne-Jones I., Learner R. C. M., Cox G., 1987, J. Phys. E, 20, 54

Thorne A. P., 1996, Phys. Scripta, T65, 31

Thorne A. P., Litzén U. & Johansson, S. 2007, in "Spectrophysics: Principles and Applications" 3rd Ed., Chapter 7.7

U.S. Naval Observatory & Royal Greenwich Observatory, "The Astronomical Almanac for the year 2014", 2013, Washington: U.S. Government Printing Office (USGPO) and London: The Stationery Office

Valenti J. A. & Piskunov N., 1996, Astron. Astrophys. Suppl. Ser., 118, 595

Volz U., Schmoranzer H., 1998, in AIP Conf. Proc. 434, "Atomic and Molecular Data and Their Applications", ed. P. J. Mohr and W. L. Wiese, Woodbury, NY:AIP, 67

Yan Z.-C., Tambasco M., Drake G. W. F., 1998, Phys. Rev. A, 57, 1652

Table 3: Experimental branching fractions, transition probabilities, and $\log(gf)$s
for the Fe I levels listed in Table 2

Lower Level (l)	$\lambda_{\mathrm{air}_{ul}}$ (Å)	σ_{ul} (cm^{-1})	BF	Δ BF (%)	A_{ul} (10^6 s^{-1})	This Experiment $\log(gf)$	$\pm$	Published $\log(gf)$	$\pm$ [1]	Ref.	GES Target?
		Level 43163.323 cm^{-1}		$3d^6 4s(^6\mathrm{D})5s$ e^{7}D$_4$	8.5 ns $\pm$ 5 %			100 % complete			
y^5F_3 *	11316.1112	8834.539	0.0010	34.2	0.117	-1.70	0.13				
y^5D_3 *	10353.2077	9656.196	0.0004	29.1	0.052	-2.13	0.11				
z^3F_4 *	8432.1889	11856.059	0.0015	19.3	0.178	-1.77	0.08				
z^5D_4	5792.6238	17263.334	0.0012	14.3	0.146	-2.18	0.06	-2.23	0.10	O'Brian et al. (1991)	
z^7P_3	5268.0211	18982.460	0.0963	0.9	11.334	-0.37	0.02	-0.39	0.03	O'Brian et al. (1991)	
z^7P_4	5140.8947	19451.867	0.0793	0.9	9.335	-0.48	0.02	-0.51	0.03	O'Brian et al. (1991)	
z^7F_3	4986.9382	20052.384	0.0115	1.5	1.349	-1.34	0.02	-1.33	0.04	O'Brian et al. (1991)	Yes
z^7F_4	4958.6820	20166.649	0.1086	0.9	12.776	-0.37	0.02	-0.41	0.03	O'Brian et al. (1991)	Yes
z^7F_5	4921.8768	20317.453	0.3082	0.7	36.260	0.07	0.02	0.07	0.03	O'Brian et al. (1991)	Yes
z^7D_3	4272.3558	23406.290	0.1559	0.8	18.345	-0.35	0.02	-0.35	0.01	Blackwell et al. (1982)	
z^7D_4	4237.1298	23600.882	0.1625	1.0	19.121	-0.34	0.02	-0.34	0.01	Blackwell et al. (1982)	
z^7D_5	4199.4872	23812.431	0.0724	0.9	8.516	-0.69	0.02	-0.72	0.01	Blackwell et al. (1982)	
		Residual	0.0012								
		Level 43633.530 cm^{-1}		$3d^6 4s(^6\mathrm{D})5s$ e^{7}D$_2$	8.4 ns $\pm$ 5 %			100 % complete			
z^7P_2	5226.8623	19126.612	0.1144	0.9	13.623	-0.55	0.02	-0.56	0.03	O'Brian et al. (1991)	
z^7P_3	5139.2515	19452.667	0.0785	0.9	9.345	-0.73	0.02	-0.74	0.03	O'Brian et al. (1991)	
z^7F_1	4903.3102	20388.693	0.0597	1.0	7.108	-0.89	0.02	-0.93	0.03	O'Brian et al. (1991)	Yes
z^7F_2	4890.7551	20441.032	0.1963	0.8	23.374	-0.38	0.02	-0.39	0.02	O'Brian et al. (1991)	
z^7F_3	4871.3182	20522.592	0.2149	0.8	25.587	-0.34	0.02	-0.36	0.02	O'Brian et al. (1991)	
z^7D_1	4233.6028	23613.894	0.1574	0.8	18.736	-0.60	0.02	-0.60	0.01	Blackwell et al. (1982)	
z^7D_3	4187.0390	23876.498	0.1776	0.8	21.138	-0.56	0.02	-0.55	0.01	Blackwell et al. (1982)	
		Residual	0.0012								
		Level 44677.003 cm^{-1}		$3d^6(^5\mathrm{D})4s(^6\mathrm{D})5s$ e^{5}D$_4$	15.4 ns $\pm$ 5 %			97 % complete			
y^5F_5	9103.6375	10981.606	0.0009	11.1	0.058	-2.19	0.05				
y^5D_4	8632.4147	11581.063	0.0007	28.5	0.048	-2.32	0.11				
z^5P_3	6400.0012	15620.679	0.1494	0.9	9.704	-0.27	0.02	-0.29	0.03	Bard et al. (1991)	Yes
z^5F_3	5784.6584	17282.313	0.0007	22.0	0.048	-2.67	0.09	-2.53	0.03	Bard et al. (1991)	Yes
z^5F_4	5709.3783	17510.184	0.0339	1.2	2.204	-1.01	0.02	-1.03	0.03	Bard et al. (1991)	
z^5F_5	5615.6439	17802.455	0.3949	0.7	25.641	0.04	0.02	0.05	0.03	Bard et al. (1991)	Yes
z^5D_3	5393.1676	18536.825	0.0753	1.0	4.888	-0.72	0.02	-0.72	0.03	Bard et al. (1991)	Yes
z^5D_4	5324.1790	18777.015	0.3133	0.8	20.341	-0.11	0.02	-0.10	0.03	Bard et al. (1991)	Yes
z^7P_3	4877.6064	20496.135						-3.09	E	May et al. (1974)	Yes
z^7P_4	4768.3965	20965.548	0.0027	10.7	0.175	-2.27	0.05	-2.46	0.06	Bard et al. (1991)	
z^7F_3	4635.6170	21566.062						-3.53	E	May et al. (1974)	
z^7F_4	4611.1849	21680.327	0.0013	39.8	0.084	-2.62	0.15	-2.72	0.08	Bard et al. (1991)	
z^7D_3	4011.7113	24919.974						-2.63	D	May et al. (1974)	
		Residual	0.0269								
		Level 47377.952 cm^{-1}		$3d^7(^4\mathrm{F})5s$ e^{5}F$_4$	19.9 ns $\pm$ 5 %			97 % complete			
y^3D_3	10863.5200	9202.598	0.0157	2.4	0.791	-0.90	0.02				
y^3F_3	9786.6450	10215.205	0.0022	8.8	0.112	-1.84	0.04				
y^3F_4	9350.4175	10691.776	0.0181	1.2	0.907	-0.97	0.02				
z^3G_4	8610.6120	11610.387	0.0041	9.2	0.205	-1.69	0.04				
z^3G_5	8331.9157	11998.744	0.1162	0.9	5.840	-0.26	0.02				
z^5G_4	8248.1309	12120.627	0.0129	10.2	0.648	-1.23	0.05				
z^5G_5	7937.1406	12595.531	0.2225	0.8	11.179	-0.02	0.02				
y^5F_3	7661.1974	13049.198	0.0328	2.3	1.650	-0.88	0.02				
y^5F_4	7495.0674	13338.435	0.2072	1.0	10.410	-0.10	0.02				
y^5F_5	7306.5623	13682.557	0.0103	6.3	0.519	-1.43	0.03				
y^5D_3	7207.3880	13870.829	0.1394	1.2	7.006	-0.31	0.02				
y^5D_4	6999.8841	14282.012	0.0124	6.1	0.625	-1.38	0.03	-1.51	D	May et al. (1974)	

[1] Data from May et al. (1974) are given the uncertainty codes 'D' and 'E' to follow the notation used by Fuhr and Wiese (2006). A letter 'D' indicates that the uncertainty is likely to be up to 50 %. A letter 'E' indicates a probable uncertainty greater than 50 % but within a factor of two in most cases. All numeric uncertainties are quoted as they appear in the source publication.

Lower Level (l)	Transition $\lambda_{\mathrm{air}_{ul}}$ (Å)	σ_{ul} (cm^{-1})	BF	Δ BF (%)	A_{ul} (10^{6}s^{-1})	This Experiment log(gf)	$\pm$	Published log(gf)	$\pm$ [1]	Ref.	GES Target?
z^5F_3	5002.7927	19983.261	0.0203	3.4	1.019	-1.46	0.03	-1.53	D	May et al. (1974)	Yes
z^5F_4	4946.3881	20211.131	0.0465	1.6	2.339	-1.11	0.02				Yes
z^5F_5	4875.8776	20503.402	0.0078	7.8	0.392	-1.90	0.04	-1.97	E	May et al. (1974)	Yes
z^5D_3	4707.2745	21237.773	0.0729	1.3	3.661	-0.96	0.02				
z^5D_4	4654.6286	21477.978	0.0309	2.4	1.553	-1.34	0.02				
		Residual	0.0278								
	Level 47960.937 cm^{-1}		$3d^7(^4\mathrm{F})5s$ e^{3}F$_4$	22.1 ns $\pm$ 5 %		98 % complete					
y^3D_3	10216.3140	9785.584	0.1176	0.9	5.320	-0.13	0.02				
y^3F_3	9258.2698	10798.191	0.0397	3.3	1.797	-0.68	0.03				
y^3F_4	8866.9329	11274.761	0.2061	0.9	9.325	-0.01	0.02				
z^3G_4	8198.9221	12193.373	0.0428	2.4	1.936	-0.76	0.02				
z^3G_5	7945.8469	12581.730	0.2589	0.8	11.717	0.00	0.02				
z^5G_5	7586.0187	13178.517	0.1514	1.0	6.849	-0.27	0.02				
y^5F_3 *	7333.5586	13632.189	0.0046	11.8	0.207	-1.82	0.05				
y^5F_4	7181.1959	13921.420	0.0248	6.0	1.121	-1.11	0.03				
y^5F_5	7007.9701	14265.533	0.0057	8.7	0.256	-1.77	0.04				
y^5D_3	6916.6815	14453.813	0.0181	6.5	0.820	-1.28	0.03	-1.40	D	May et al. (1974)	
z^3F_3	6725.3572	14864.995	0.0029	24.4	0.131	-2.10	0.10				Yes
y^5D_4	6187.9904	16155.865						-1.67	E	May et al. (1974)	
z^3D_3	6008.5566	16638.324	0.0478	2.2	2.165	-0.98	0.02				Yes
z^3F_4	6003.0123	16653.691	0.0366	2.9	1.655	-1.10	0.02				Yes
z^5F_3	4860.9785	20566.245	0.0032	18.2	0.146	-2.33	0.08	-2.38	E	May et al. (1974)	
z^5F_4	4807.7088	20794.117	0.0050	12.3	0.226	-2.15	0.05	-2.15	D	May et al. (1974)	
z^5F_5	4741.0696	21086.389	0.0029	16.6	0.131	-2.40	0.07				
z^5D_3	4581.5080	21820.760	0.0114	6.4	0.517	-1.83	0.03	-1.78	D	May et al. (1974)	
		Residual	0.0205								
	Level 48702.532 cm^{-1}		$3d^6(^3\mathrm{H})4s4p(^3\mathrm{P}^o)$ y^{1}G$_4^o$	21.0 ns $\pm$ 5 %		96 % complete					
c^3F_4	6315.8115	15828.901	0.0093	26.3	0.441	-1.63	0.10	-1.66	D	May et al. (1974)	Yes
b^1G_4	5288.5247	18903.605	0.0181	2.9	0.862	-1.49	0.02	-1.51	0.04	O'Brian et al. (1991)	Yes
b^3D_3	5171.6731	19330.718	0.0031	24.7	0.148	-2.27	0.10				
a^1H_5	5028.1264	19882.579	0.0593	1.8	2.825	-1.02	0.02	-1.12	0.04	O'Brian et al. (1991)	Yes
b^3H_4	4528.7570	22074.924	0.0072	7.0	0.344	-2.02	0.04	-1.99	0.07	O'Brian et al. (1991)	
a^1G_4	4143.4146	24127.879	0.5620	1.0	26.762	-0.21	0.02	-0.20	0.04	O'Brian et al. (1991)	
b^3G_4	4066.5852	24583.714	0.0226	8.1	1.075	-1.62	0.04	-1.58	0.04	O'Brian et al. (1991)	
a^3G_3	3779.2027	26453.094	0.0038	19.9	0.181	-2.46	0.08				
a^3G_4	3743.7765	26703.405						-2.17	0.08	O'Brian et al. (1991)	
a^3G_5	3704.4612	26986.800	0.2740	1.8	13.047	-0.62	0.02	-0.58	0.04	O'Brian et al. (1991)	
b^3F_3	3592.4702	27828.059						-2.42	E	May et al. (1974)	
a^3F_4	2722.0390	36726.287						-2.20	0.05	O'Brian et al. (1991)	
		Residual	0.0406								
	Level 51294.217 cm^{-1}		$3d^6(^5\mathrm{D})4s(^4\mathrm{D})5s$ e^{3}D$_3$	9.9 ns $\pm$ 5 %		97 % complete					
y^3D_3	7620.5128	13118.865	0.0467	3.0	4.712	-0.54	0.03				
y^5P_2 *	7071.8713	14136.631	0.0129	35.1	1.301	-1.17	0.13				
y^3F_4	6843.6560	14608.042	0.0374	5.7	3.780	-0.73	0.03	-0.89	D	May et al. (1974)	Yes
y^5F_4	5793.9148	17254.703						-1.66	E	May et al. (1974)	Yes
z^3P_2	5762.9922	17347.286	0.1229	2.6	12.412	-0.36	0.02	-0.47	D	May et al. (1974)	
y^5D_3	5620.4924	17787.098						-1.75	E	May et al. (1974)	
y^5D_4	5493.4988	18198.279	0.0104	20.3	1.053	-1.48	0.08	-1.80	E	May et al. (1974)	
z^3F_3	5129.6308	19489.150	0.0077	16.6	0.780	-1.67	0.07	-1.81	E	May et al. (1974)	Yes
z^3D_2	5098.5723	19607.869	0.0478	2.1	4.826	-0.88	0.02				
z^3D_3	5005.7123	19971.606	0.2837	1.1	28.661	-0.12	0.02				
z^3F_4	5001.8636	19986.973	0.3722	1.1	37.598	-0.01	0.02	-0.01	D	May et al. (1974)	Yes
z^5F_4	4143.4972	24127.398	0.0185	20.9	1.865	-1.47	0.09	-2.14	E	May et al. (1974)	
z^5D_3	3974.3807	25154.037	0.0079	31.8	0.796	-1.88	0.12	-1.86	E	May et al. (1974)	

[1] Data from May et al. (1974) are given the uncertainty codes 'D' and 'E' to follow the notation used by Fuhr and Wiese (2006). A letter 'D' indicates that the uncertainty is likely to be up to 50 %. A letter 'E' indicates a probable uncertainty greater than 50 % but within a factor of two in most cases. All numeric uncertainties are quoted as they appear in the source publication.

Lower Level (l)	Transition $\lambda_{\mathrm{air}_{ul}}$ (Å)	σ_{ul} (cm^{-1})	BF	Δ BF (%)	A_{ul} (10^{6}s^{-1})	This Experiment log(gf)	$\pm$	Published log(gf)	$\pm$ [1]	Ref.	GES Target?
		Residual	0.0319								
	Level 51461.667 cm^{-1}			$3d^64s(^6$D$)4d$ f^{5}F$_4$	12.7 ns $\pm$ 5 %		87 % complete				
w^5D_3	13260.7300	7539.001						-0.64	0.06	O'Brian et al. (1991)	
x^5F_3	9414.0422	10619.516	0.0575	2.3	4.524	-0.27	0.02	-0.32	0.13	O'Brian et al. (1991)	
x^5F_4	9199.4455	10867.238	0.0084	9.5	0.661	-1.12	0.04				
x^5D_3	8699.4540	11491.818	0.0535	2.0	4.216	-0.37	0.02	-0.38	0.13	O'Brian et al. (1991)	Yes
x^5D_4	8446.5685	11835.875	0.0048	33.6	0.377	-1.44	0.13				
z^5P_3	4461.9698	22405.338	0.0286	7.0	2.253	-1.22	0.04	-1.21	0.03	O'Brian et al. (1991)	
z^5F_3	4153.8997	24066.978	0.2872	1.1	22.612	-0.28	0.02	-0.32	0.02	O'Brian et al. (1991)	
z^5F_4	4114.9376	24294.850	0.0196	9.3	1.545	-1.45	0.04	-1.45	0.06	O'Brian et al. (1991)	
z^5D_3	3948.0973	25321.490	0.1542	2.3	12.140	-0.59	0.02	-0.56	0.03	O'Brian et al. (1991)	
z^5D_4	3910.9991	25561.674						-1.26	0.06	O'Brian et al. (1991)	
z^7P_3	3664.5374	27280.804	0.0585	3.8	4.607	-1.08	0.03	-1.07	0.03	O'Brian et al. (1991)	
z^7F_3	3526.2380	28350.730	0.2021	2.1	15.915	-0.57	0.02	-0.55	0.02	O'Brian et al. (1991)	
z^7D_3	3153.1997	31704.637						-0.97	0.03	O'Brian et al. (1991)	
		Residual	0.1256								
	Level 51770.554 cm^{-1}			$3d^6(^5$D$)4s(^4$D$)5s$ g^{3}D$_3$	12.1 ns $\pm$ 5 %		92 % complete				
x^5F_3	9147.9579	10928.402	0.0187	6.2	1.548	-0.87	0.03				
x^5F_4	8945.1900	11176.124	0.0843	3.0	6.963	-0.23	0.03				
x^5D_3	8471.7444	11800.702	0.0199	5.4	1.649	-0.91	0.03				
y^5P_2	6841.3391	14612.989	0.0795	4.6	6.568	-0.49	0.03	-0.78	D	May et al. (1974)	Yes
y^5P_3	6663.2325	15003.588	0.0164	27.6	1.358	-1.20	0.11				
y^3F_4	6627.5448	15084.378	0.0067	25.6	0.556	-1.59	0.10				Yes
y^5F_2	5804.4627	17223.348						-2.01	E	May et al. (1974)	
y^5F_3	5731.7623	17441.803						-1.27	D	May et al. (1974)	
y^5F_4	5638.2621	17731.040	0.0692	2.9	5.716	-0.72	0.02	-0.84	D	May et al. (1974)	Yes
y^5D_2	5563.6002	17968.983	0.0662	8.4	5.470	-0.75	0.04	-0.96	D	May et al. (1974)	
y^5D_3	5473.9005	18263.434	0.0740	3.4	6.113	-0.72	0.03	-0.79	D	May et al. (1974)	Yes
y^5D_4	5353.3736	18674.616	0.0706	3.7	5.831	-0.76	0.03				
z^3D_3	4889.1021	20447.943	0.0311	6.0	2.570	-1.19	0.03				
z^3F_4	4885.4306	20463.310	0.0519	3.7	4.287	-0.97	0.03				Yes
z^5P_2	4482.7393	22301.531	0.0208	12.8	1.718	-1.44	0.06	-1.32	E	May et al. (1974)	
z^5P_3	4401.2899	22714.232	0.0616	3.5	5.090	-0.99	0.03	-0.89	D	May et al. (1974)	
z^5F_3	4101.2611	24375.865	0.0306	13.7	2.531	-1.35	0.06	-1.35	D	May et al. (1974)	
z^5F_4	4063.2757	24603.737	0.1082	3.2	8.942	-0.81	0.03				
z^5D_2	3931.1172	25430.861	0.0420	30.6	3.469	-1.25	0.12	-1.11	E	May et al. (1974)	
z^5D_3	3900.5150	25630.379	0.0685	9.7	5.665	-1.04	0.05	-0.90	D	May et al. (1974)	
		Residual	0.0798								
	Level 52039.889 cm^{-1}			$3d^6(^5$D$)4s(^4$D$)5s$ e^{3}D$_1$	10.4 ns $\pm$ 5 %		87 % complete				
x^5F_1	9163.9826	10909.292	0.0074	13.8	0.710	-1.57	0.06				
y^3D_1	7664.1587	13044.156	0.0166	29.7	1.594	-1.38	0.11				
y^3F_2	6885.7564	14518.727						-1.35	E	May et al. (1974)	
z^3P_0	5717.8329	17484.293	0.0780	4.9	7.502	-0.96	0.03	-1.10	D	May et al. (1974)	Yes
y^5D_1	5546.9924	18022.782						-1.88	E	May et al. (1974)	
y^5D_2	5481.4387	18238.318	0.0364	8.8	3.499	-1.33	0.04	-1.42	E	May et al. (1974)	
z^3F_2	5022.2355	19905.900	0.4292	1.5	41.267	-0.33	0.02	-0.56	D	May et al. (1974)	Yes
z^3D_1	4973.1019	20102.565	0.1906	3.2	18.331	-0.69	0.03	-0.92	D	May et al. (1974)	
z^3D_2	4911.7794	20353.538	0.0170	17.1	1.630	-1.75	0.07	-1.76	D	May et al. (1974)	
z^5P_1	4481.6093	22307.154	0.0368	13.1	3.534	-1.50	0.06	-1.39	D	May et al. (1974)	
z^5F_2	4083.7632	24480.307	0.0535	8.2	5.147	-1.41	0.04				
		Residual	0.1345								
	Level 52067.446 cm^{-1}			$3d^6(^5$D$)4s(^6$D$)4d$ e^{5}P$_2$	14.3 ns $\pm$ 5 %		77 % complete				
x^5F_3	8905.9947	11225.310	0.0144	9.4	1.010	-1.22	0.04				

[1] Data from May et al. (1974) are given the uncertainty codes 'D' and 'E' to follow the notation used by Fuhr and Wiese (2006). A letter 'D' indicates that the uncertainty is likely to be up to 50 %. A letter 'E' indicates a probable uncertainty greater than 50 % but within a factor of two in most cases. All numeric uncertainties are quoted as they appear in the source publication.

Lower Level (l)	Transition $\lambda_{\mathrm{air}_{ul}}$ (Å)	σ_{ul} (cm^{-1})	BF	Δ BF (%)	A_{ul} (10^{6}s^{-1})	This Experiment log(gf)	±	Published log(gf)	±[1]	Ref.	GES Target?
x^5D_1	8571.8052	11662.950	0.0201	8.9	1.408	-1.11	0.04				Yes
x^5D_2	8446.3844	11836.133	0.0320	9.6	2.240	-0.92	0.05				
y^5P_1	6820.3719	14657.912						-1.29	E	May et al. (1974)	Yes
y^5P_2	6705.1024	14909.899	0.0576	9.2	4.024	-0.87	0.04				Yes
y^5P_3	6533.9294	15300.499						-1.43	E	May et al. (1974)	Yes
y^5F_3	5635.8226	17738.715						-1.86	E	May et al. (1974)	
z^3P_2	5517.0655	18120.544						-2.34	E	May et al. (1974)	
y^5D_1	5538.5162	18050.364	0.0179	14.1	1.252	-1.54	0.06				Yes
y^5D_2	5473.1642	18265.891						-2.11	E	May et al. (1974)	
y^5D_3	5386.3341	18560.342						-1.74	E	May et al. (1974)	
z^3F_3	4933.8730	20262.397	0.0215	11.9	1.503	-1.56	0.05				
z^3D_2	4905.1328	20381.117	0.0147	24.7	1.026	-1.73	0.10	-2.02	E	May et al. (1974)	Yes
z^5P_1	4476.0755	22334.732	0.4386	1.5	30.671	-0.34	0.02				
z^5P_2	4423.8408	22598.446	0.0241	10.9	1.686	-1.61	0.05	-1.58	D	May et al. (1974)	
z^5P_3	4344.4995	23011.142	0.0714	4.3	4.995	-1.15	0.03				
z^5F_2	4079.1681	24507.883	0.0214	28.8	1.498	-1.73	0.11	-1.17	E	May et al. (1974)	
z^5F_3	4051.9053	24672.778	0.0379	16.7	2.647	-1.49	0.07	-1.40	D	May et al. (1974)	
		Residual	0.2284								

Lower Level (l)	Transition $\lambda_{\mathrm{air}_{ul}}$ (Å)	σ_{ul} (cm^{-1})	BF	Δ BF (%)	A_{ul} (10^{6}s^{-1})	This Experiment log(gf)	±	Published log(gf)	±[1]	Ref.	GES Target?
	Level 54683.318 cm^{-1}		$3d^7(^4$F$)4d$ f^{3}F$_4$		23.5 ns ± 5 %	92 % complete					
y^3D_3	6056.0047	16507.966	0.2295	3.4	9.768	-0.32	0.03				Yes
y^3F_3	5705.9922	17520.575	0.1838	3.4	7.821	-0.46	0.03	-0.57	D	May et al. (1974)	
y^3F_4	5554.8951	17997.142	0.3059	2.2	13.016	-0.27	0.02				Yes
z^3G_3	5373.7086	18603.949	0.1187	3.7	5.050	-0.71	0.03	-0.84	D	May et al. (1974)	Yes
z^3G_4	5285.1286	18915.752	0.0138	35.9	0.586	-1.66	0.13	-1.62	E	May et al. (1974)	Yes
z^3G_5	5178.8006	19304.114						-1.82	E	May et al. (1974)	
z^5G_4	5146.3064	19426.000						-2.01	E	May et al. (1974)	
z^5G_5	5023.4978	19900.898	0.0146	19.5	0.623	-1.67	0.08	-1.69	E	May et al. (1974)	Yes
y^5F_3	4911.5294	20354.574	0.0105	19.2	0.447	-1.84	0.08	-2.22	E	May et al. (1974)	
y^5D_3 *	4720.9645	21176.188	0.0109	18.5	0.464	-1.86	0.08				
z^3F_3 *	4369.7269	22878.296	0.0143	50.2	0.608	-1.81	0.18				
z^3D_3	4279.4887	23360.704						-1.44	D	May et al. (1974)	
z^3D_3	4276.6761	23376.067	0.0170	37.9	0.723	-1.75	0.14	-1.19	D	May et al. (1974)	
		Residual	0.0810								

[1] Data from May et al. (1974) are given the uncertainty codes 'D' and 'E' to follow the notation used by Fuhr and Wiese (2006). A letter 'D' indicates that the uncertainty is likely to be up to 50 %. A letter 'E' indicates a probable uncertainty greater than 50 % but within a factor of two in most cases. All numeric uncertainties are quoted as they appear in the source publication.

Table 4: Lines measured in previous studies, or predicted to have a BF greater than 1%, that were omitted from the BF measurements shown in Table 3

Lower Level (l)	Transition $\lambda_{\mathrm{air}_{ul}}$ (Å)	σ_{ul} (cm^{-1})	Published log(gf)	±[1]	Ref.	Predicted BF	Reason for Omission	Probable Blends
	Level 44677.003 cm^{-1}		$3d^6(^5$D$)4s(^6$D$)5s$ e^{5}D$_4$		15.4 ns ± 5 %	97 % complete		
y^5P_3	12638.7060	7910.038	-0.774		Kurucz (2007)	0.0107	Outside Range	
z^7P_3	4877.6064	20496.135	-3.090	E	May et al. (1974)	0.0003	Not observed	
z^7F_3	4635.6170	21566.062	-3.530	E	May et al. (1974)	0.0001	Not observed	
z^7D_3	4011.7113	24919.974	-2.630	D	May et al. (1974)	0.0015	Not observed	
					Sum	0.0126		
	Level 47960.937 cm^{-1}		$3d^7(^4$F$)5s$ e^{3}F$_4$		22.1 ns ± 5 %	98 % complete		
z^3F_3	6187.9904	16155.865	-1.670	E	May et al. (1974)	0.0097	Not observed	
					Sum	0.0097		

[1] Data from May et al. (1974) are given the uncertainty codes 'D' and 'E' to follow the notation used by Fuhr and Wiese (2006). A letter 'D' indicates that the uncertainty is likely to be up to 50 %. A letter 'E' indicates a probable uncertainty greater than 50 % but within a factor of two in most cases. All numeric uncertainties are quoted as they appear in the source publication.

Lower Level (l)	$\lambda_{\mathrm{air}_{ul}}$ (Å)	σ_{ul} (cm^{-1})	$\log(gf)$	$\pm$ [1]	Ref.	Predicted BF	Reason for Omission	Probable Blends
					Level 48702.532 cm^{-1} $3d^6(^3\mathrm{H})4s4p(^3\mathrm{P}^o)$ y^{1}G$_4^o$ 21.0 ns $\pm$ 5 % 96 % complete			
y^1G_4	3743.7765	26703.405	-2.170	0.08	O'Brian et al. (1991)	0.0077	Not observed	
y^1G_4	3592.4702	27828.059	-2.420	E	May et al. (1974)	< 0.0001	Not observed	
y^1G_4	2722.0390	36726.287	-2.200	0.05	O'Brian et al. (1991)	0.0137	Not observed	
					Sum	0.0214		
					Level 51294.217 cm^{-1} $3d^6(^5\mathrm{D})4s(^4\mathrm{D})5s$ e^{3}D$_3$ 9.9 ns $\pm$ 5 % 97 % complete			
y^5F_4	5793.9148	17254.703	-1.660	E	May et al. (1974)	0.0023	Too weak to fit	
y^5D_3	5620.4924	17787.098	-1.750	E	May et al. (1974)	0.0022	Too weak to fit	
					Sum	0.0045		
					Level 51461.667 cm^{-1} $3d^6 4s(^6\mathrm{D})4d$ f^{5}F$_4$ 12.7 ns $\pm$ 5 % 87 % complete			
w^5D_3	13260.7300	7539.001	-0.642	0.06	O'Brian et al. (1991)	0.0097	Outside Range	
z^5D_4	3910.9991	25561.674	-1.257	0.06	O'Brian et al. (1991)	0.0211	Too weak to fit	
z^7D_3	3153.1997	31704.637	-0.974	0.03	O'Brian et al. (1991)	0.0800	Blended	Unknown[2]
					Sum	0.1108		
					Level 51770.554 cm^{-1} $3d^6(^5\mathrm{D})4s(^4\mathrm{D})5s$ g^{5}D$_3$ 12.1 ns $\pm$ 5 % 92 % complete			
y^5F_2	5804.4627	17223.348	-2.010	E	May et al. (1974)	0.0041	Not observed	
y^5F_3	5731.7623	17441.803	-1.270	D	May et al. (1974)	0.0165	Not observed	
z^3P_2	5608.9723	17823.630	-1.493		Kurucz (2007)	0.0144	Not observed	
					Sum	0.0350		
					Level 52039.889 cm^{-1} $3d^6(^5\mathrm{D})4s(^4\mathrm{D})5s$ e^{3}D$_1$ 10.4 ns $\pm$ 5 % 87 % complete			
y^3F_2	6885.7564	14518.727	-1.350	E	May et al. (1974)	0.0090	Blended	Fe II: λ_{air} = 6885.779 Å
								Fe II: λ_{air} = 6885.825 Å
z^3P_1	5655.4900	17677.028	-0.796		Kurucz (2007)	0.0794	Blended	Fe I: λ_{air} = 5655.490 Å
y^5D_1	5546.9924	18022.782	-1.880	E	May et al. (1974)	0.0068	Not observed	
z^5D_0 *	4481.6073	25489.422	-2.472		Kurucz (2007)	0.0104	Not observed	
					Sum	0.1056		
					Level 52067.446 cm^{-1} $3d^6(^5\mathrm{D})4s(^6\mathrm{D})4d$ e^{5}P$_2$ 14.3 ns $\pm$ 5 % 77 % complete			
y^5P_1	6820.3719	14657.912	-1.290	E	May et al. (1974)	0.0634	Too weak to fit	
y^5F_3	5635.8226	17738.715	-1.860	E	May et al. (1974)	0.0035	Not observed	
z^3P_2	5517.0655	18120.544	-2.340	E	May et al. (1974)	0.0017	Not observed	
y^5D_2	5473.1642	18265.891	-2.110	E	May et al. (1974)	0.0030	Not observed	
y^5D_3	5386.3341	18560.342	-1.740	E	May et al. (1974)	0.0051	Not observed	
z^5D_1 *	3906.9605	25588.097	-1.467		Kurucz (2007)	0.0426	Not observed	
z^5D_2 *	3885.7475	25727.782	-1.285		Kurucz (2007)	0.0393	Not observed	
z^5D_3	3855.8454	25927.298	-1.296		Kurucz (2007)	0.0278	Not observed	
					Sum	0.1864		
					Level 54683.318 cm^{-1} $3d^7(^4\mathrm{F})4d$ f^{3}F$_4$ 23.5 ns $\pm$ 5 % 92 % complete			
z^3G_5	5178.8006	19304.114	-1.820	E	May et al. (1974)	0.0068	Not observed	
z^5G_4	5146.3064	19426.000	-2.010	E	May et al. (1974)	0.0054	Not observed	
z^3D_3	4279.4887	23360.704	-1.440	D	May et al. (1974)	0.0373	Not observed	
z^3F_4	4276.6761	23376.067	-1.355		Kurucz (2007)	0.0354	Too weak to fit	
					Sum	0.0849		

[1] Data from May et al. (1974) are given the uncertainty codes 'D' and 'E' to follow the notation used by Fuhr and Wiese (2006). A letter 'D' indicates that the uncertainty is likely to be up to 50 %. A letter 'E' indicates a probable uncertainty greater than 50 % but within a factor of two in most cases. All numeric uncertainties are quoted as they appear in the source publication.

[2] The line at 31704.637 cm^{-1} was observed to be significantly stronger than expected. Its inclusion in the BF measurements resulted in serious disagreement with published values for all lines belonging to the 51461.667 cm^{-1} upper level.

Table 5. Lines from Table 3 selected for solar synthesis.

λ_{air} (Å)	χ_{lower} (eV)	VdW [a] Parameter	This experiment log(gf)	$\pm$	Previously Published log(gf)	$\pm$ [b]	Ref.	log[ϵ(Fe)] This experiment	Previous work
4423.8408	3.654	933.274	-1.61	0.05	-1.58	D	May et al. (1974)	7.43	7.40
4807.7088	3.368	904.227	-2.15	0.05	-2.15	D	May et al. (1974)	7.56	7.56
5001.8636	3.882	725.240	-0.01	0.02	-0.01	D	May et al. (1974)	7.41	7.41
5022.2355	3.984	742.238	-0.33	0.02	-0.56	D	May et al. (1974)	7.43	7.66
5285.1286	4.435	1046.282	-1.66	0.13	-1.62	E	May et al. (1974)	7.60	7.56
5373.7086	4.473	1044.282	-0.71	0.03	-0.76	D	May et al. (1974)	7.40	7.45
5393.1676	3.241	791.237	-0.72	0.02	-0.72	0.03	Bard et al. (1991)	7.44	7.44
5473.9005	4.154	738.241	-0.72	0.03	-0.79	D	May et al. (1974)	7.48	7.55
5538.5162	4.218	-7.480	-1.54	0.06	-3.24		Kurucz (2007)	7.49	9.19
5615.6439	3.332	794.241	0.04	0.02	0.05	0.03	Bard et al. (1991)	7.45	7.44
5638.2621	4.220	730.235	-0.72	0.02	-0.84	D	May et al. (1974)	7.42	7.54
5717.8329	4.284	758.209	-0.96	0.03	-1.10	D	May et al. (1974)	7.50	7.64
5784.6584	3.397	796.244	-2.67	0.09	-2.53	0.03	Bard et al. (1991)	7.55	7.41
6003.0123	3.882	898.241	-1.10	0.02	-1.12		Kurucz (2007)	7.58	7.61
6056.0047	4.733	1029.286	-0.32	0.03	-0.46		Kurucz (2007)	7.38	7.52
6315.8115	4.076	410.250	-1.63	0.10	-1.61		Kurucz (2007)	7.48	7.47
6400.0012	3.603	802.252	-0.27	0.02	-0.29	0.03	Bard et al. (1991)	7.42	7.44
6627.5448	4.549	754.209	-1.59	0.10	-1.58		Kurucz (2007)	7.57	7.56
6705.1024	4.607	-7.480	-0.87	0.04	-1.39		Kurucz (2007)	7.31	7.83
6725.3572	4.103	897.241	-2.10	0.10	-2.01		Kurucz (2007)	7.36	7.28
6841.3391	4.607	759.267	-0.49	0.03	-0.78	D	May et al. (1974)	7.25	7.54
6843.6560	4.549	736.216	-0.73	0.03	-0.83	D	May et al. (1974)	7.38	7.48
6916.6815	4.154	901.243	-1.28	0.03	-1.40	D	May et al. (1974)	7.46	7.58
6999.8841	4.103	845.244	-1.38	0.03	-1.46	D	May et al. (1974)	7.46	7.54
7007.9701	4.178	903.244	-1.77	0.04	-1.96		Kurucz (2007)	7.37	7.56
7306.5623	4.178	846.244	-1.43	0.03	-1.43		Kurucz (2007)	7.35	7.35
7661.1974	4.256	-7.550	-0.88	0.02	-0.83		Kurucz (2007)	7.52	7.47
8571.8052	5.010	-7.480	-1.11	0.04	-1.41		Kurucz (2007)	7.48	7.78
8610.6120	4.435	-7.550	-1.69	0.04	-2.65		Kurucz (2007)	7.41	8.37
8699.4540	4.956	-7.510	-0.37	0.02	-0.38	0.13	O'Brian et al. (1991)	7.41	7.42
8905.9947	5.064	-7.480	-1.22	0.04	-3.65		Kurucz (2007)	7.45	9.88
8945.1900	5.033	-7.530	-0.23	0.03	-0.23		Kurucz (2007)	7.46	7.46
9103.6375	4.178	-7.540	-2.19	0.05	-1.96		Kurucz (2007)	7.53	7.30
9199.4455	5.033	-7.510	-1.12	0.04	-1.01		Kurucz (2007)	7.30	7.19
9786.6450	4.608	-7.550	-1.84	0.04	-1.68		Kurucz (2007)	7.46	7.30
10863.5200	4.733	-7.550	-0.90	0.02	-0.90		Kurucz (2007)	7.45	7.45

[a] Van der Waals broadening parameter. Values greater than zero were obtained from Anstee, Barklem & O'Mara (ABO) theory (Anstee & O'Mara 1991, 1995) and are expressed in the standard packed notation where the integer component is the broadening cross section, σ, in atomic units, and the decimal component is the dimensionless velocity parameter, α. Values less than zero are the log of the VdW broadening parameter, γ_6 (rad s^{-1}), per unit perturber number density, N (cm^{-3}), at 10000 K (i.e. log[γ_6/N] in units of rad s^{-1} cm^3). These were used only when ABO data were unavailable. See Gray (2005) for more details.

[b] Data from May et al. (1974) are given the uncertainty codes 'D' and 'E' to follow the notation used by Fuhr and Wiese (2006). A letter 'D' indicates that the uncertainty is likely to be up to 50 %. A letter 'E' indicates a probable uncertainty greater than 50 % but within a factor of two in most cases. All numeric uncertainties are quoted as they appear in the source publication.